Politecnico di Torino

Master of Science in Energy and Nuclear Engineering

01FJIXY - Computational Thermomechanics

A.Y. 2025/2026

Homework 06 - 2D Thermal Problem

Tommaso COGOZZO
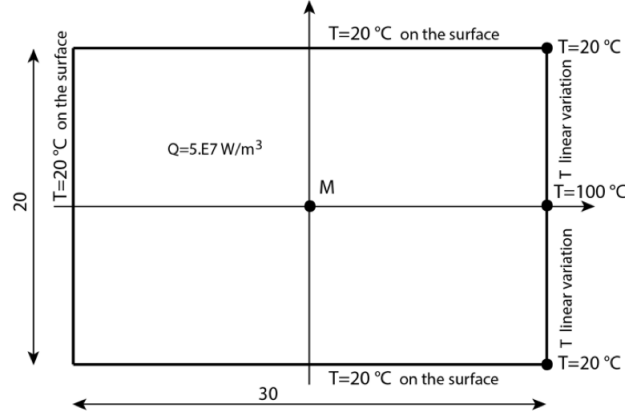
1 Problem statement and given data

Figure 1: conducting rod of rectangular cross section with a uniform heat generation inside and imposed temperatures at the boundaries

Data:

- Length: $L = 10\,m$

- Height: $h = 1\,m$

- Thermal conductivity: $k = 1.0\,W/(mK)$

- Heat source: $Q = 5.0 \times 10^7\,W/(m^3)$

2 Objective

The objective of this essay is to perform a numerical investigation of the steady-state heat conduction problem in a rectangular conducting rod with uniform internal heat generation, subjected to prescribed temperature boundary conditions. The analysis is carried out using the finite element method implemented in the Finite Elements Analysis Program.

Different two dimensional finite element discretizations are considered, including linear triangular and rectangular elements, as well as selected higher order elements, in order to assess the influence of mesh type and refinement on the accuracy of the computed temperature field. Exploiting the geometric and thermal symmetry of the problem, the temperature distribution is evaluated with particular attention to the horizontal symmetry axis, and the temperature value at the midpoint of the rod is monitored.

A progressive mesh refinement strategy is adopted to study the convergence behavior of the numerical solution, comparing the evolution of the midpoint temperature for increasingly refined discretizations. Finally, keeping the boundary

conditions unchanged, the internal heat generation is adjusted to determine the value required to achieve a target temperature of 300 °C at the midpoint of the domain (M).

The results are presented in terms of temperature distributions, heat flux contours, and quantitative comparisons, providing a comprehensive assessment of the thermal response of the system and the numerical performance of the adopted finite element models.

3 Finite Element Analysis with 3-Nodes Triangular Elements

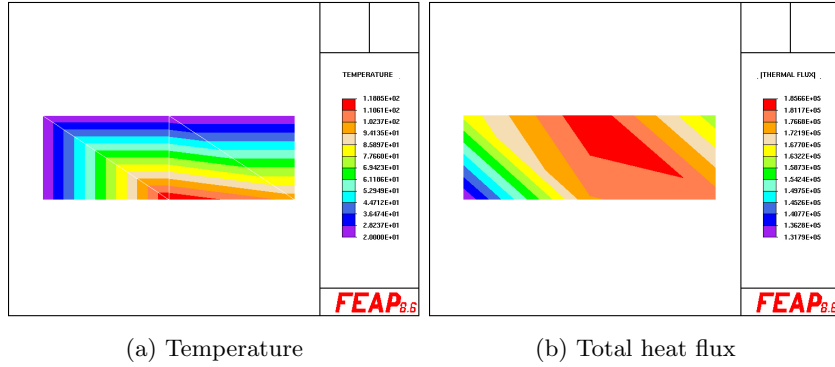(a) Temperature   (b) Total heat flux

Figure 2: Computed temperature and total heat flux with nodal increment =1

Exploiting the symmetry of the problem with respect to the horizontal (x) axis, the computational domain is discretized using four three node triangular finite elements. The resulting temperature field and heat flux distribution obtained from this coarse discretization are shown in Figure 2.

With regard to the heat flux, it should be noted that the quantity reported in the aforementioned figure represents the total heat flux magnitude, obtained by combining the contributions along the x and y directions. For the sake of clarity and to allow a more detailed interpretation of the thermal behavior, the individual heat flux components along the two coordinate directions are presented separately in Figure 3.

At the right vertical boundary $(x = L = 1.5 \times 10^{-2}\,\mathrm{m})$, a prescribed temperature distribution with pyramidal (linear) variation along the y-direction is imposed. Restricting the analysis to the upper half-domain, the temperature varies linearly from

$$T = 100\ ^{\circ}\mathrm{C} \quad \text{at} \quad y = 0 \tag{1}$$

to

$$T = 20\ ^{\circ}\mathrm{C} \quad \text{at} \quad y = h/2 = 1.0 \times 10^{-2}\,\mathrm{m}. \tag{2}$$

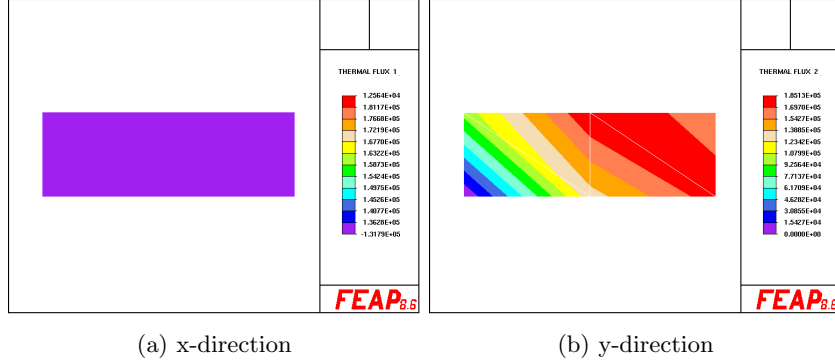(a) x-direction   (b) y-direction

Figure 3: Computed x-directed heat flux and y-directed

The resulting temperature gradient along the y-direction at the right boundary is therefore

$$\frac{\partial T}{\partial y} = \frac{20 - 100}{1.0 \times 10^{-2}} = -8.0 \times 10^3 \, °\text{C/m}. \tag{3}$$

Applying Fourier's law, the heat flux component along the y-direction in proximity of the right boundary is given by

$$q_y = -k\frac{\partial T}{\partial y}. \tag{4}$$

Substituting the material property $k = 20 \, \text{W/(m°C)}$, one obtains

$$q_y = -20 \times (-8.0 \times 10^3) = 1.6 \times 10^5 \, \text{W/m}^2. \tag{5}$$

The positive sign indicates an upward heat flux, consistent with heat flowing from the hotter region near the symmetry axis toward the colder upper surface.

At the right boundary, the temperature is prescribed (Dirichlet condition). As a consequence, the temperature gradient normal to the boundary cannot be directly inferred from the boundary condition alone. However, due to the strong temperature constraint and the absence of a sharp temperature variation in the vicinity of the boundary along the x-direction, the local temperature gradient $\partial T/\partial x$ is expected to be smaller than the gradient along y.

Therefore, in proximity of the right boundary, the heat flux component along the x-direction can be reasonably assumed to be negligible compared to q_y:

$$q_x = -k\frac{\partial T}{\partial x} \approx 0. \tag{6}$$

The analytical evaluation highlights that, near the right boundary, the heat transfer mechanism is dominated by the vertical temperature gradient imposed by the pyramidal boundary condition. The heat flux is therefore primarily oriented along the y-direction, while the contribution along the x-direction is

marginal. This observation is consistent with the numerical results obtained using a coarse discretization, where limited variation of the heat flux along y may indicate insufficient mesh resolution to accurately capture the imposed thermal gradient.
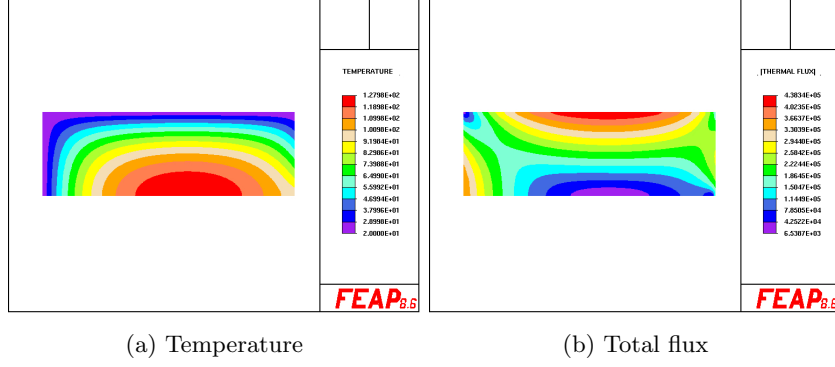

(a) Temperature

(b) Total flux

Figure 4: Computed temperature and heat flux (mr: 256x32)

After several numerical implementations involving progressively refined meshes, the solution obtained using a mesh resolution of mr $= 256 \times 32$ is selected for the final analysis. The corresponding results, in terms of temperature distribution and heat flux field, are reported in Figure 4.

In particular, inspection of Figure 4a shows that the temperature values at the four corners of the computational domain are in full agreement with the prescribed boundary conditions provided in the problem statement. This consistency indicates that the adopted mesh refinement is sufficiently fine to accurately capture the imposed thermal constraints, thereby confirming the reliability and accuracy of the numerical results.
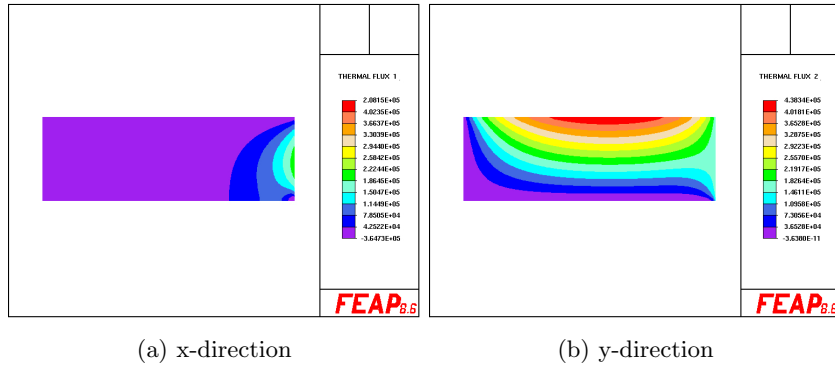

(a) x-direction

(b) y-direction

Figure 5: Computed x-directed heat flux and y-directed

In order to better assess the results related to the heat flux field, the total

heat flux is once again decomposed into its Cartesian components. In this case, a non negligible gradient is observed along both spatial directions.

Along the x-direction, the heat flux exhibits a pronounced peak in the vicinity of the right boundary, in agreement with the problem data and the imposed temperature conditions. At the same time, a significant variation of the heat flux is also detected along the y-direction, reflecting the presence of a vertical temperature gradient induced by the non-uniform boundary temperature distribution.

Moreover, the smoothness and spatial consistency of the heat flux contours obtained with the finest mesh provide clear evidence of numerical convergence. In particular, further mesh refinements do not lead to appreciable variations in either the magnitude or the spatial distribution of the heat flux components, indicating that the finite element solution has reached a mesh independent regime and can therefore be considered converged.
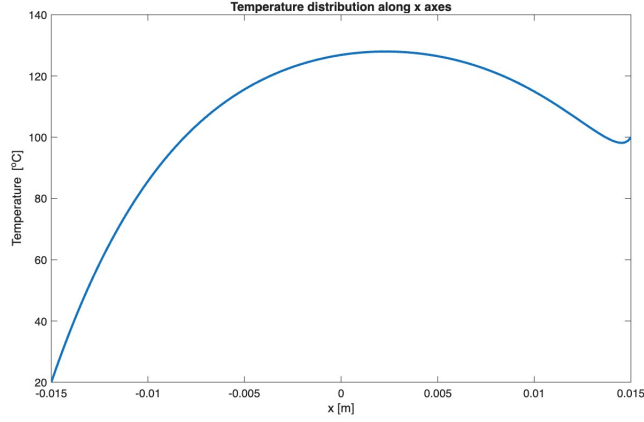

Figure 6: Computed temperature distribution along x axes

Finally, Figure 6 reports the graphical distribution of the temperature along the x-axis. As expected, the temperature profile exhibits a curvilinear behavior due to the presence of internal heat generation. Moreover, the temperature values at the domain boundaries coincide with those prescribed in the problem data, consistently with what was previously observed in the colormap representation. In addition, the temperature at point M, with coordinates $(0,0)$, can be evaluated and is found to be equal to $1.2687 \times 10^2 \, °\mathrm{C}$.

4 Finite Element Analysis with 4-Nodes Rectangular Elements

The FEM analysis of the 2D thermal problem is thus repeated using linear rectangular elements. As before, the results are examined in terms of temperature

distribution and heat flux, considering a coarser discretization with $m_r = 2 \times 1$. The data obtained are presented in Figure 7.
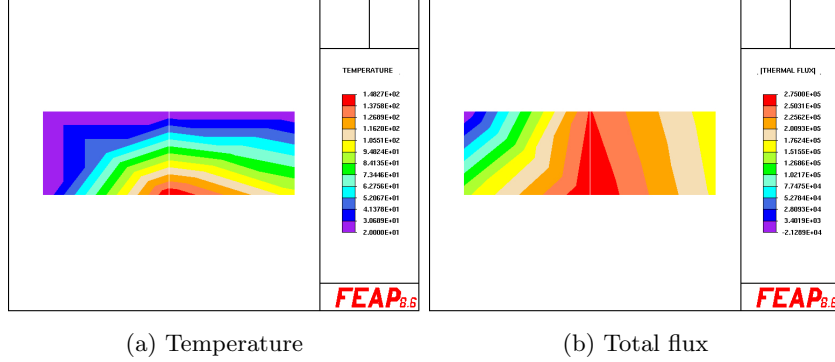

(a) Temperature   (b) Total flux

Figure 7: Computed temperature and heat flux (mr: 2x1)

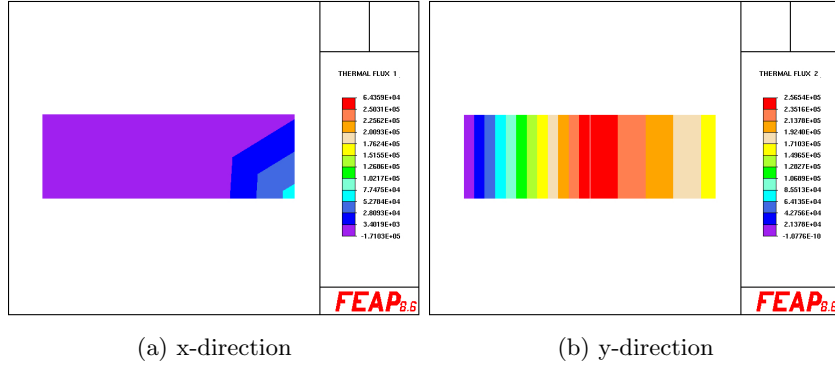(a) x-direction   (b) y-direction

Figure 8: Computed x-directed heat flux and y-directed

Although the results from this initial implementation appear significantly more accurate than those obtained with the first implementation using triangular elements, particularly when comparing Figure 8a and 3a they still remain limited and far from the expected outcome. In this case as well, the heat flux in the y-direction exhibits a negligible thermal gradient, which is entirely inconsistent with the expected behavior, given that the problem data indicate a substantial temperature difference between the two boundaries.

Observation of the temperature distribution along the x-axis, shown graphically in Figure 9, further indicates that a finer discretization is required to achieve more accurate results. Although the temperature values at the domain boundaries (also visible in Figure 7a) are consistent with the problem specifications, the overall qualitative trend deviates from the expected behavior.

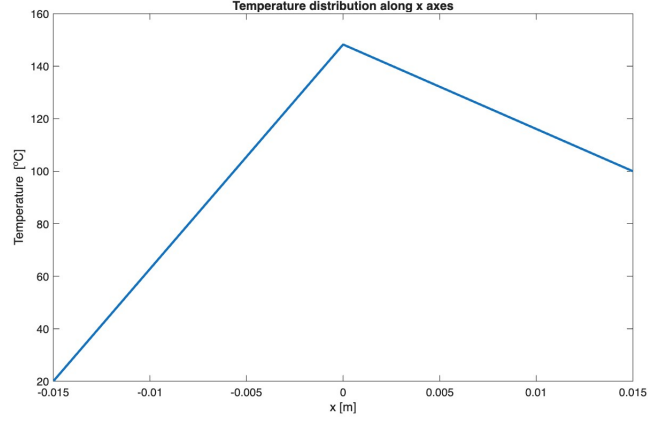After a series of implementations with progressively finer mesh refinements,

6

Figure 9: Computed temperature distribution along x axes (mesh = 2x1)

the final result is achieved using a discretization of $m_r = 256 \times 32$, as was done in Section 3. The reliability of the obtained results is confirmed by a heat flux distribution that is fully consistent with the boundary conditions along both the vertical and horizontal edges of the examined subdomain. Furthermore, the temperature distribution along the coordinate axis $(x, 0)$ exhibits a qualitative behavior and extreme values that are in excellent agreement with the prescribed boundary data. This demonstrates that the chosen discretization is sufficient to accurately capture the thermal gradients and overall behavior of the system.
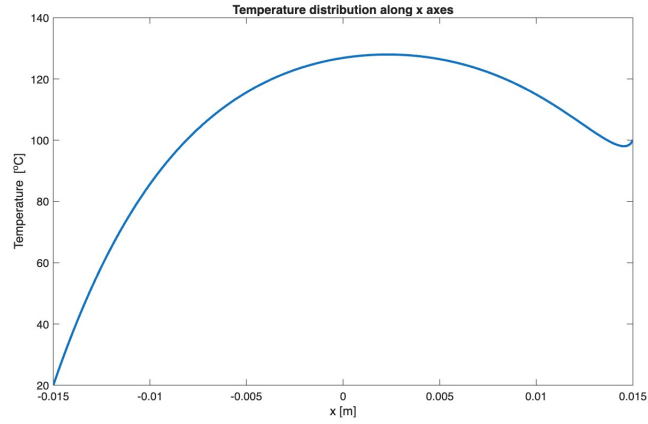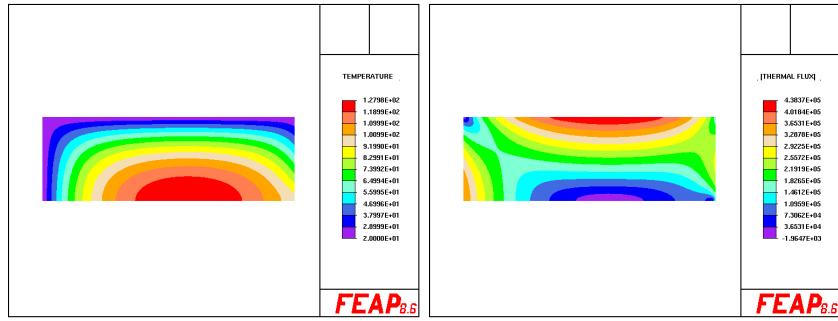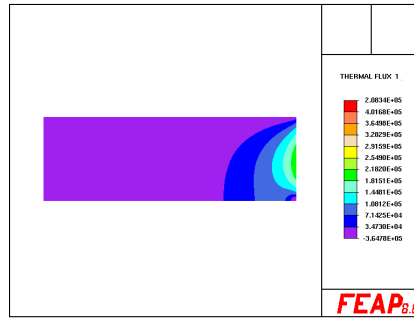

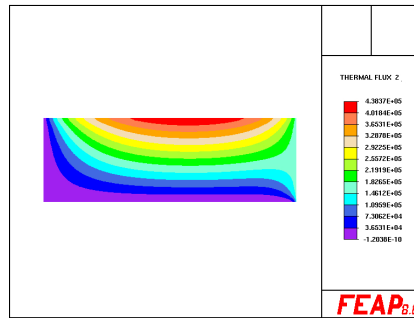Figure 10: Computed temperature distribution along x axes (mesh = 256x32)

7

(a) Temperature

(b) Total flux

(c) x-direction

(d) y-direction

Figure 11: Computed temperature and heat flux (mr: 256x32)

5   Determination of the Heat Generation Required to Reach $T_M = 300$ °C

The value of the volumetric heat generation, q, required to achieve a temperature of 300 °C at point M was determined numerically using a discretization with linear rectangular elements and a mesh of 256×32. By adjusting the heat generation in each implementation and monitoring the temperature at point M (which can be observed using the command "disp, , (ih+1)*i1+1"), the target temperature of 300 °C was obtained when $q = 1.36 \times 10^8$ W/m^3. For completeness, the same procedure was repeated using linear triangular elements, and similarly, the same value of q led to the desired temperature at point M, confirming the consistency of the numerical approach across different element types.

However, a second interesting aspect emerges when the mesh refinement is reduced. Using three-node triangular elements with a mesh of 128×32 and the previously calculated heat generation value ($q = 1.36 \times 10^8$ W/m^3), the temperature at point M is approximately 294 °C. This observation leads to the conclusion that the temperature at any point in the domain depends on both the mesh refinement and the chosen discretization strategy. Nonetheless, for a given mesh, no significant differences have been observed between triangular and rectangular elements, indicating that both element types provide comparable accuracy under the same discretization density.

6 Conclusions

This study presented a comprehensive numerical investigation of steady-state heat conduction in a rectangular rod with uniform internal heat generation, subjected to prescribed temperature boundary conditions. Both linear triangular (three-node) and rectangular (four-node) finite elements were employed to discretize the computational domain, and a progressive mesh refinement strategy was implemented to assess convergence and solution accuracy.

The analysis highlighted several important findings. First, the temperature distributions and heat flux fields obtained with the finest discretization ($m_r = 256 \times 32$) are in excellent agreement with the prescribed boundary conditions, confirming that the adopted mesh resolution is sufficient to accurately capture the thermal gradients and overall behavior of the system. The decomposition of the heat flux into Cartesian components revealed that the flux is predominantly oriented along the direction of the steepest temperature gradient, while smooth and spatially consistent contours indicate numerical convergence.

Second, the determination of the volumetric heat generation necessary to achieve a target temperature at the midpoint, $T_M = 300$ °C, demonstrated the robustness of the numerical approach. Both triangular and rectangular elements yielded consistent results, with $q = 1.36 \times 10^8$ W/m^3 required to reach the desired temperature at M. Nevertheless, a reduction in mesh refinement leads to lower midpoint temperatures, emphasizing the influence of both mesh density and element type on the accuracy of local temperature predictions. Importantly, for a given discretization, differences between triangular and rectangular elements were minimal, indicating comparable performance in capturing the thermal response.

Overall, this investigation confirms that a carefully refined finite element model is essential to achieve reliable and physically consistent predictions in two-dimensional heat conduction problems. The results provide a clear demonstration of mesh convergence, discretization effects, and the interplay between numerical resolution and boundary-driven thermal behavior, offering valuable guidance for the design and analysis of thermally sensitive systems.